RESEARCH ARTICLE | OCTOBER 06 2025

A postbuckling-based metamaterial for switching the propagation of surface acoustic waves

F. Aloschi ; F. Zeighami ; A. Palermo ; C. Daraio

Appl. Phys. Lett. 127, 141701 (2025)
https://doi.org/10.1063/5.0297652
CHORUS

Applied Physics Letters ARTICLE pubs.aip.org/aip/apl

A postbuckling-based metamaterial for switching the propagation of surface acoustic waves

Cite as: Appl. Phys. Lett. **127**, 141701 (2025); doi: 10.1063/5.0297652
Submitted: 20 August 2025 · Accepted: 6 September 2025 ·
Published Online: 6 October 2025

F. Aloschi,[1,2,a)] F. Zeighami,[3] A. Palermo,[3] and C. Daraio[1]

AFFILIATIONS

[1]Division of Engineering and Applied Science, California Institute of Technology, Pasadena, California 91125, USA
[2]Department of Mechanical Engineering, University of Colorado Boulder, Boulder, Colorado 80309, USA
[3]Department of Civil, Chemical, Environmental and Materials Engineering, University of Bologna, Bologna 40136, Italy

[a)]Author to whom correspondence should be addressed: fabrizioaloschi@gmail.com

ABSTRACT

The use of periodic materials for wave control and signal processing has been a focus of intensive research over the past two decades and continues to garner significant attention. Common signal processing mechanisms like switches and rectifiers often depend on magnetic fields and/or logic gates for their activation. We propose a metamaterial that enables the control of mechanical waves—surface acoustic waves—through an ON–OFF mechanism that switches the propagation of the waves through a tunable platform of elastic beams. In the OFF configuration, the beams remain in their undeformed state and resonate at a specific frequency range, creating a bandgap that stops wave propagation. Conversely, in the ON configuration, the beams undergo buckling, redistributing the vibration energy across multiple modes and eliminating the bandgap, thus allowing wave propagation. Analytical and numerical findings demonstrate the significant potential of this mechanism for controlling wave propagation in nonlinear periodic materials. This switching mechanism relies purely on mechanical processes, thereby eliminating the need for external fields.

Wave manipulation through periodic materials has been successful in various fields,[1–3] including the control of surface acoustic waves (SAWs).[4–8] Material and geometric nonlinearities have been utilized to exploit phenomena such as localization,[9] breathers,[10] bifurcation, and chaos.[11] The postbuckling regime offers a significant source of nonlinearity due to its ease of realization and inherently reversible nature. Indeed, the ability to transition between prebuckling and postbuckling states without inducing plastic deformation enables enhanced control and versatility in the system's mechanical response. Leveraging this concept, our approach proposes a strategy for manipulating SAWs using buckling-prone elastic slender beams, attached to the surface of an elastic substrate, that act as longitudinal resonators. Typically, phononic materials with periodic arrays of standing substructures are constructed using non-slender bulky resonators[12] to enhance wave mode localization effects.[13] On the other hand, slender beams might be preferred for achieving sub-wavelength bandgaps,[14] or for controlling low-frequency surface[15,16] and flexural waves.[17–19] Here, the choice of slender beams helps reach buckling before encountering local damage or plasticity.

Two conceptual diagrams in Fig. 1 illustrate the switching mechanism activated by the proposed metamaterial. As depicted in Figs. 1(a) and 1(b), the slender monolithic beams are rigidly constrained at the top, and intentionally designed to have axial modes within the frequency range of SAWs.

In the prebuckling configuration, shown in Fig. 1(c), where no compressive force is applied, the axial resonance of the beams generates a low-frequency bandgap, corresponding to the OFF state. The application of external compression beyond the critical load, combined with a small initial geometrical imperfection common to all beams, causes buckling and softening,[20] as depicted in Fig. 1(d). This is achieved by applying a small initial lateral force to promote buckling in a specific direction, thereby preventing bifurcation and avoiding the pounding effect between adjacent beams in the array configuration. Buckling shifts the resonance frequency and reduces the peak amplitude of the frequency response function (FRF) corresponding to the fundamental mode of the beams. As a result, the buckled configuration activates the ON state of the metamaterial, eliminating the bandgap within the frequency range of interest and enabling SAW transmission.

To demonstrate the underlying physics of the switching mechanism, an array of identical beams is periodically placed on an elastic

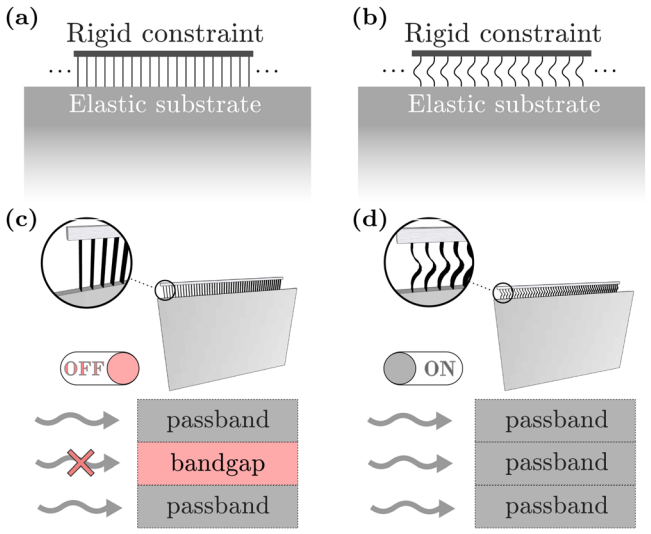

FIG. 1. Array of periodically distributed mechanical resonator beams in (a) prebuckling and (b) postbuckling states. Conceptual diagrams of the switching mechanism for (c) OFF and (d) ON configuration.

substrate with uniform spacing. The beams and substrate are made of poly(methyl methacrylate) (PMMA) material with a mass density of $\rho = 1190\,\mathrm{kg/m^3}$, Poisson's ratio of $\nu = 0.4$, and Young's modulus of $E = 3 \times 10^9$ Pa. A damping ratio of 0.1% is assumed for the beams. Without loss of generality, a 2D model of the switch system is considered, where each beam has a length of $l_b = 11d$ and a thickness of $h_b = d/27$, with $d = 0.008$ m representing the spacing between adjacent beams. The beams are slender, satisfying $l_b > 50h_b$. The substrate has a length of $n_b \times d$, where n_b denotes the number of beams, and a height of $5\lambda_0$, with λ_0 being the reference wavelength at resonance.

Two-dimensional finite element (FE) models are developed under the plane-stress assumption in COMSOL Multiphysics[21] to evaluate the static and dynamic response of a single isolated beam. Then, surface acoustic wave propagation in the mechanical switch is investigated by analyzing the dispersion relation of the metamaterial using a semi-analytical approach. Finally, a full numerical model of the switch device is developed to validate the dispersion results obtained from the semi-analytical approach.

The numerical investigation begins with a nonlinear buckling analysis of a single beam subjected to a progressively increasing axial load, P. In the developed numerical model, the beam is clamped at both ends and discretized using triangular mesh elements with a maximum element size of $h_b/2$. Figure 2(a) presents the buckling results for a slender clamped-clamped beam, showing the imposed axial load normalized by the Euler critical load, $P_{cr} = 0.79$ N, as a function of the longitudinal displacement normalized by the tip vertical displacement, v_0. For completeness, the numerical FE simulations are compared with the results obtained by the Elastica model[22] in Fig. 2(a), which provides an upper bound of the postbuckling equilibrium path associated with the beam with no imperfections, see details in the supplementary material of this article.

We replicate the analysis by applying a progressively increasing vertical displacement v_0. In the displacement-driven buckling analysis,

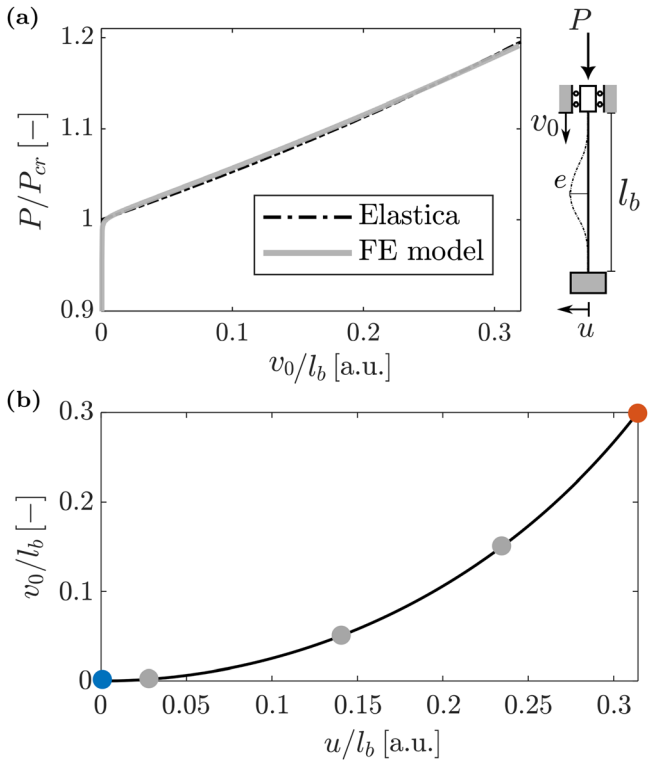

FIG. 2. Single axially loaded clamped beam: (a) load-displacement diagram in the vicinity of the Euler critical load and (b) vertical–horizontal displacement graph in the postbuckling configuration, with circles representing the v_0 values investigated in the vibration analysis of Fig. 3.

the beam is buckled by applying a horizontal force that introduces a very small eccentricity, $e = 10^{-4}\,l_b$, at the midpoint of the beam. The required force is calculated as $F = 192EIe/l_b^3$, where I is the second moment of inertia of the beam.[23] Figure 2(b) depicts the imposed vertical displacement v_0 plotted against the horizontal displacement in the middle of the beam, u, with both displacements normalized by the beam length l_b. The blue and orange dots correspond to the OFF and ON states, respectively.

Next, a harmonic analysis is carried out for both the prebuckling and the linearized postbuckling states. The latter is performed to evaluate the dynamic response of the buckled beam for small vibrations around the postbuckled equilibrium configuration. In both cases, we compute the axial force, i.e., the vertical reaction force, at the bottom constraint of the beam under an imposed harmonic longitudinal displacement applied at the top. The results are shown in Fig. 3(a), where the vertical reaction force, R_y, at the base is normalized by the corresponding value obtained in the static, prebuckling regime, $R_{y0,p}$, i.e., at $f = 0$ Hz. In the linear prebuckling regime at $v_0 = 0$, resonance frequencies correspond to the normal modes of the beam, and are given by the general expression $f_{n,j} = j\frac{c_{B,b}}{2l_b}$, where j is the mode number and $c_{B,b} = \sqrt{E/\rho}$ is the longitudinal wave speed of the beam. The two observed peaks in Fig. 3(a) correspond to the first and second modes, $f_{n,1}$ and $f_{n,2}$, which are obtained by substituting $j = 1, 2$, respectively. The speed of longitudinal wave propagation depends on the ratio of

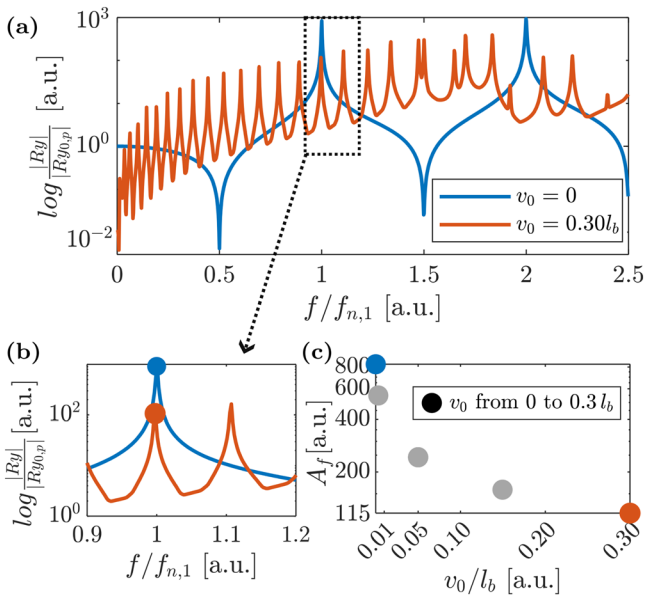

FIG. 3. FRF of the longitudinal vibrations of the clamped-clamped beam: (a) reaction force R_y at the base of the beam, (b) zoom in the vicinity of the first normal mode $f/f_{n,1} = 1$, and (c) FRF peaks at $f/f_{n,1} = 1$ for several values of imposed vertical displacement v_0.

the beam's Young modulus E to its mass density ρ: neither the area nor the cross section influences it. For thin beams, this assumption is valid for those frequencies that are sufficiently low, such that the wavelengths are much greater than the cross-sectional dimensions.

In the postbuckling state, the reaction force at the beam's base decreases significantly with increasing v_0, as shown in Fig. 3(b), and additional peaks emerge corresponding to different coupled axial-flexural vibration modes of the buckled beam. The FRF peaks associated with the first fundamental longitudinal mode of the prebuckling state, called A_f, decrease significantly, leading to negligible force transfer to the base in the frequency range of interest. Since wave propagation across a periodic array of beams attached to a substrate is governed by the forces exchanged at their interface,[16] the reaction forces obtained here can be directly correlated with the dispersion characteristics of the mechanical switch. In particular, we focus on the axial force exchanged near the first longitudinal resonance of the beam, as shown in the zoomed Fig. 3(b), and track the variation of the resonance peak, A_f, under different imposed displacements. Note that $A_f = log\frac{|Ry|}{|R_{y0,p}|}$ evaluated at $f = f_{n,1}$. Figure 3(c) shows that A_f decreases by about 85% from the prebuckled configuration, $v_0 = 0$, to the desired buckled configuration, $v_0 = 0.3 l_b$. We anticipate that, in the buckled configuration, the reaction force from postbuckling vibrations is too low to interact with the SAW propagation, and therefore, no bandgap formation is anticipated, as demonstrated in the following section. Additionally, we remark that at $v_0 = 0.3 l_b$ the beam stress remains below the material's ultimate strength, thereby preventing material failure or fracture during buckling.

Building on the single-beam analyses, the dispersion characteristics of a periodic array of unbuckled and buckled beams attached to the substrate are analyzed using a semi-analytical dispersion model, as

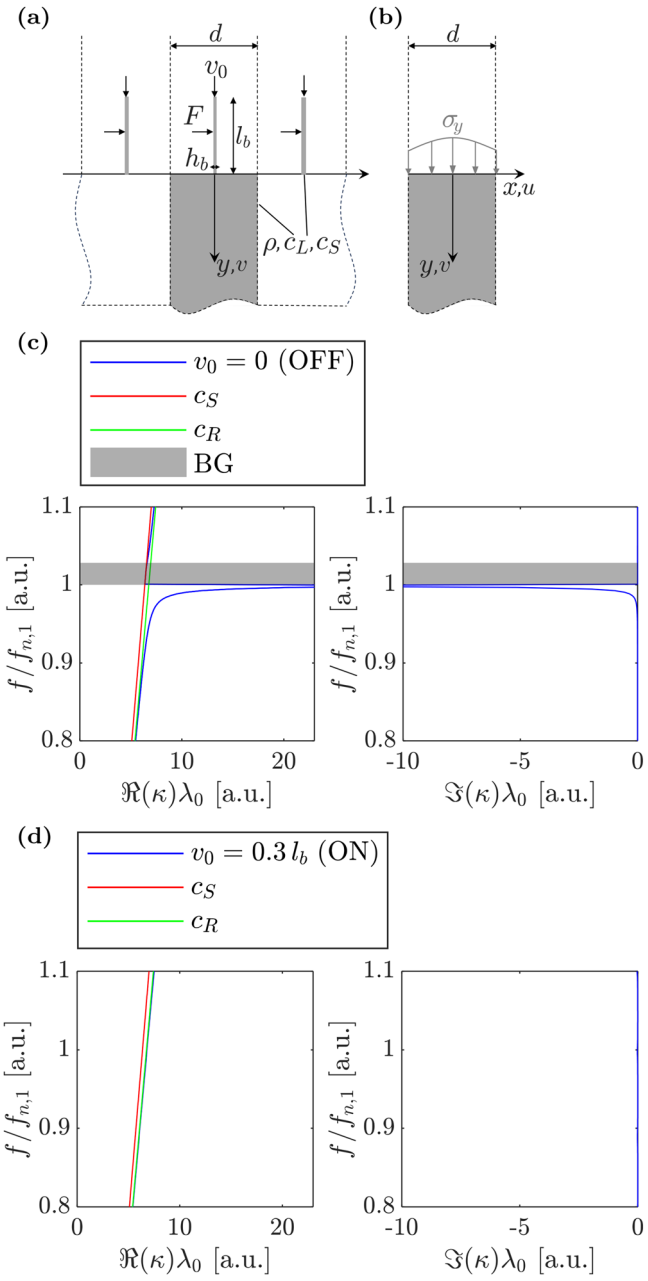

FIG. 4. Schematics of the unit cell used for the dispersion analysis: (a) continuous beam, (b) vertical stress transmitted from the beams to the substrate, and used for deriving the analytical dispersion relation. Panels (c) and (d) show the SAW dispersion relations for the OFF and ON configurations, respectively, including both the real and imaginary parts of the wavenumber. The bandgap (BG) region is highlighted with a gray box in (c).

schematically illustrated in Fig. 4(a). The formulation is derived based on the sub-wavelength regime assumption, where both the beam dimensions and their spacing are significantly smaller than the SAW wavelength. Under this condition, the array of beams exerts a distributed vertical stress, σ_y, on the elastic substrate, as shown in Fig. 4(b).

The long-wavelength approximation holds for both the OFF and ON states of the device and enables a simplified yet accurate description of the SAW–structure interaction, forming the basis for a semi-analytical dispersion model. The dispersion relation reads as follows:[24]

$$\left(2-\frac{\omega^2}{k^2c_S^2}\right)^2-4\sqrt{1-\frac{\omega^2}{k^2c_L^2}}\sqrt{1-\frac{\omega^2}{k^2c_S^2}}=-\frac{\sigma_y\,\omega^2}{\rho\,c_S^4\,k^3}\sqrt{1-\frac{\omega^2}{k^2c_L^2}}, \tag{1}$$

where ω is the angular frequency, k is the wavenumber, ρ is the mass density, and c_L and c_S are the longitudinal and shear wave speeds of the substrate. The vertical stress, $\sigma_y = R_y/A_b$, is computed from the vertical reaction force R_y at the base of each beam, obtained from the FRF analysis presented in Fig. 3(a), and averaged over the beam cross section area.

The dispersion relation is solved numerically by inputting the frequency values extracted from the FRF plots and computing the corresponding complex wavenumber using `fsolve`, a Newton-type root-finding algorithm implemented in MATLAB.[25] Consequently, the dispersion curves for the OFF and ON configurations are obtained, as shown in Figs. 4(c) and 4(d), respectively. In the dispersion plots, the frequency is normalized by $f_{n,1}$, and the wavenumber is normalized as $k\lambda_0$, where $\lambda_0 = c_R/f_{n,1}$, and c_R denotes the surface Rayleigh wave velocity. The results indicate that, in the OFF configuration, where the beams remain in the prebuckling state, the fundamental SAW mode strongly couples with the substrate at resonance, as it asymptotically approaches $f_{n,1}$. This coupling gives rise to a low-frequency bandgap, highlighted by the gray region in Fig. 4(c), which emerges from the collective local longitudinal resonance of the beams. The limits of the bandgap frequency range can be estimated using an equivalent lumped-mass model of the beam coupled to the substrate,[26] as $f_{\mathrm{BG}} = \left[f_{n,1},\, f_{n,1}\left(\beta+\sqrt{\beta^2+1}\right)\right]$, where $\beta = \frac{m_b f_{n,1}\pi}{\rho c_S d}\sqrt{1-\left(\frac{c_S}{c_L}\right)^2}$ and m_b is the mass of a single beam. The presence of this bandgap is further confirmed by the imaginary part of the dispersion plot, which exhibits significant attenuation within the bandgap frequency range, with a peak attenuation occurring at $f_{n,1}$.

The dispersion plots of the ON configuration is shown in Fig. 4(d), where the beams are in the buckled state. The postbuckling condition is achieved by imposing a displacement of $v_0 = 0.3l_b$ at the tip of the beam, and the dispersion relation is obtained by inserting the corresponding reaction force, obtained from the FRF analysis of Fig. 3, into Eq. (1). In this case, the bandgap is closed, and the surface waves propagate with a velocity close to the Rayleigh wave speed. No attenuation is observed in the imaginary part of the wavenumber, indicating wave transmission within the bandgap frequency range of the undeformed beams. This behavior is attributed to the reduced amount of stress exerted by the buckled beams on the substrate in the ON configuration, as previously observed in Fig. 3(b). Indeed, when the transmitted stress is small, the term on the right-hand side of the dispersion relation in Eq. (1) becomes negligible, and the dispersion law recovers the classical form of Rayleigh wave propagation.[27] In other words, the interaction between the beam and the SAW remains too weak to generate a local resonance bandgap.

The proposed ON–OFF switching mechanism is now tested on a full numerical model developed in COMSOL Multiphysics. In more detail, a two-dimensional FE model is developed under plane-stress conditions, with a height of $H_m = 5\lambda_0$ and a length of $L_m = 40\lambda_0$, as shown in Fig. 5(a). A harmonic source is placed at a distance of $2\lambda_0$ from the right edge of the model and $8\lambda_0$ away from the switching device to excite the system and generate SAWs. This buffer zone is considered to avoid near-source effects and ensure clean surface wave propagation before reaching the beam array. The latter consists of $n_b = 253$ beams with uniform spacing d periodically arranged on the substrate for an overall length of $20\lambda_0$. The array size is considered to be sufficiently large to provide adequate spatial resolution, enabling an accurate reconstruction of the dispersion curves. The two bottom corners of the model are fixed, and perfectly matched layers (PMLs) of thickness λ_0 are applied to the bottom and lateral boundaries to prevent back reflections from these boundaries. The beams are discretized using the same mesh type and size adopted in the FRF analysis. The substrate is meshed with triangular elements: in the upper region of the model, with a height of λ_0, where most of the SAW energy is concentrated, the mesh size is set to $d_{\mathrm{mesh}} = [0.5d,\, d]$; in the remaining part of the substrate, a coarser mesh is used with $d_{\mathrm{mesh}} = [d,\, 5d]$.

Harmonic frequency response analysis is performed on the normalized frequency interval $(0.5 - 1.5)$, targeting the frequency range near the first resonance of the beam, with a resolution of $\Delta f = f_{n,1}/1000$. A total of 1000 observation points are equally distributed within the beam array, at the top of the substrate, from which vertical nodal displacements are extracted. Three case studies are analyzed: (i) a pristine plate without beams, (ii) a plate equipped with undeformed beams in the OFF configuration, and (iii) a plate with buckled beams in the ON configuration. For the ON case, the analysis is conducted in two steps. First, a static analysis is carried out to buckle the beams progressively from $v_0 = 0$ to $v_0 = 0.3l_b$. Then, we perform a frequency-domain analysis under the assumption of small vibrations, linearizing the problem around the buckled equilibrium configuration. To reconstruct the dispersion curves, a spatial Fourier transform (FT) is applied to the nodal displacements extracted from the observation points within the beam array. It is noted that, for the ON configuration, the displacements induced by the static buckling analysis are removed before performing the harmonic analysis, in order to highlight the wave propagation associated solely with the harmonic source.

The reconstructed dispersion relations are shown in the background of Figs. 5(b)–5(d) for the pristine plate, the OFF, and the ON configurations, respectively. For the pristine plate, the analytical Rayleigh wave dispersion law,[28] obtained by setting zero vertical stress, i.e., $\sigma_y = 0$, in Eq. (1), is superimposed on the figure. For comparison, in both OFF and ON configurations of the metamaterial, the semi-analytical dispersion curves shown in Figs. 4(c) and 4(d) are added to the dispersion plots as solid blue lines. The dynamic interaction between the beam array and the soft substrate lowers the resonance frequency of the coupled system, resulting in a corrected resonance value below the intrinsic longitudinal resonance of the beam. This corrected frequency is expressed as $f_c = \alpha f_{n,1}$, where $\alpha < 1$ denotes the resonance frequency correction coefficient. The derivation and implementation of this coefficient are provided in the supplementary material.

In all three cases, good agreements are observed between the numerical and reference results. In the OFF configuration, the beams

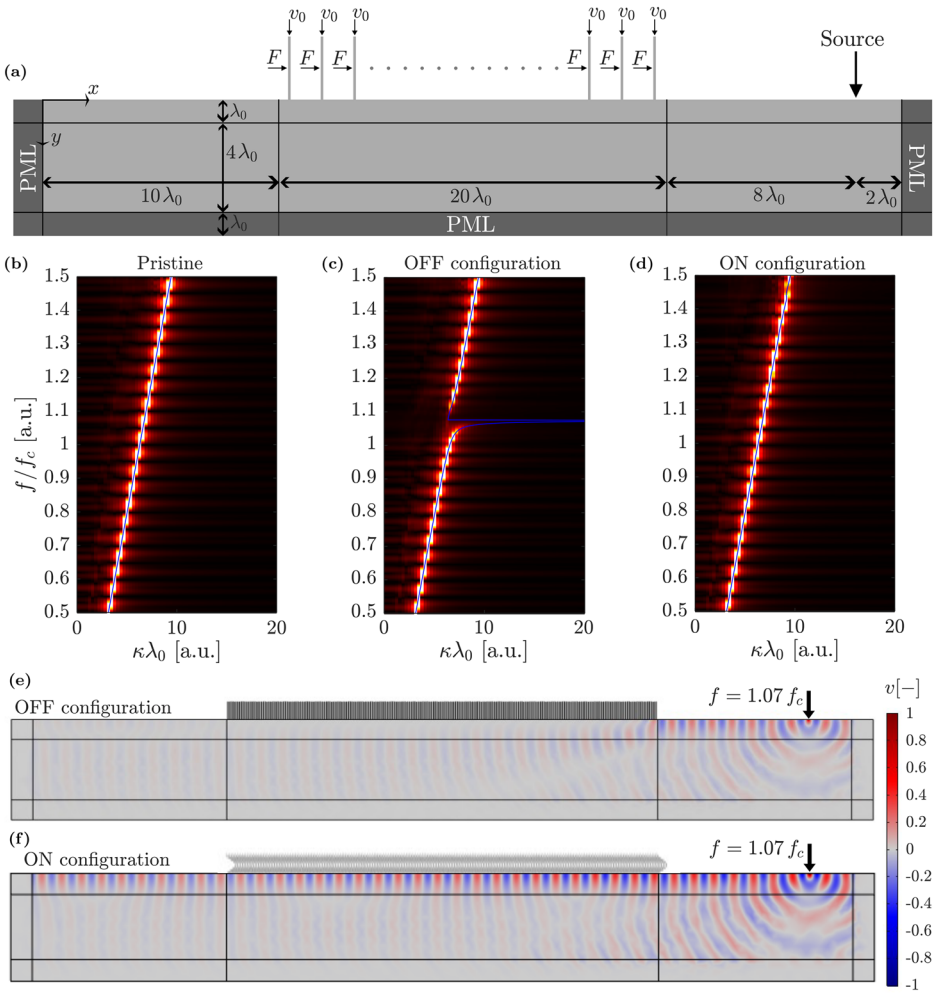

FIG. 5. (a) Schematic representation of the FE model of the mechanical switching device. SAW dispersion curves for (b) pristine plate without beams, (c) OFF configuration with beams in the prebuckling state, and (d) ON configuration with beams in the postbuckling state. The background of the dispersion plots in (b)–(d) corresponds to the spatial Fourier transform of the harmonic simulations performed in COMSOL Multiphysics, whereas blue curves are the relevant semi-analytical dispersions obtained from Eq. (1). Panels (e) and (f) display the vertical displacement wavefields, v, under harmonic excitation at $f = 1.07\, f_c$ for the OFF and ON configurations, respectively.

in their undeformed state resonate, and the excitation of the lowest-order axial mode leads to the formation of a low-frequency bandgap, thereby realizing the switching-OFF functionality of the device, as shown in Fig. 5(c). In contrast, in the ON state shown in Fig. 5(d), when the beams are axially compressed, the force exchanged between the array of beams and the substrate is significantly reduced. As a result, SAWs propagate through the metamaterial with minimal disturbance in the frequency range $0.9f_c$–$1.2f_c$, resembling the behavior of the pristine plate case shown in Fig. 5(b). These simulations are further validated using a wave finite element model (WFEM) of the single unit cell under plane-stress conditions. Good agreement is observed among the WFEM, the harmonic analysis, and the semi-analytical model for both ON and OFF configurations. However, for the sake of brevity, the WFEM results are reported and described in detail in the supplementary material. The efficiency of the proposed device is further illustrated through the vertical displacement wavefield, obtained by exciting the model at $f = 1.07f_c$, a frequency located within the bandgap of the OFF configuration. The results show that, when a SAW impinges on the array of beams in the OFF state, wave propagation is impeded and surface-to-shear wave conversion occurs, a phenomenon previously observed in the interaction of surface waves with elastic metasurfaces.[26,29] In contrast, in the ON configuration, the SAWs propagate undisturbed through the array.

In conclusion, we have proposed a metamaterial for a mechanically actuated switching mechanism that enables or suppresses the propagation of SAWs within desired frequency ranges. In the ON configuration, the system uses an array of buckled slender beams on an elastic substrate, whose softening behavior suppresses bandgaps and enables SAW transmission. The dispersive properties of the metamaterial device are analyzed through a semi-analytical approach validated through full FE numerical simulations. SAWs devices are widely used to convert electrical signals into mechanical waves and vice versa, with applications in sensors, MEMS, and filters. Our approach is well suited for SAW devices, offering the advantage of purely mechanical activation without the need for external electromagnetic fields, thus facilitating practical implementation. As a final remark, we note that the filtering performance of the proposed device can be further enhanced by applying the concept of rainbow trapping, i.e., by varying the beam lengths over a broad range, to achieve an extended bandgap in the OFF configuration.

See the supplementary material for the concise explanation of the Elastica model used in this study along with details on the WFEM implementation, which was employed to further verify the switching mechanism of the proposed metamaterial, but was omitted from the main article for brevity.

This work was partially supported by the Science and Technology Center New Frontiers of Sound (NewFoS) through NSF Grant No. 2242925 (C.D.). F.Z. acknowledges the funding received from the Italian Ministry of Education, Universities, and Research (MUR) for the "ELeMEnT" project (Grant Agreement SOE0000157, CUP: J53C22003890002), under "Young Researchers Call 2022" of the National Recovery and Resilience Plan (NRRP) funded by the European Union—NextGenerationEU. A.P. acknowledges the funding received from the Italian Ministry of University and Research (MUR) for the "EXTREME" project (Grant Agreement 2022EZT2ZE, CUP: J53C24002870006).

AUTHOR DECLARATIONS

Conflict of Interest

The authors have no conflicts to disclose.

Author Contributions

F. Aloschi: Conceptualization (lead); Data curation (equal); Formal analysis (equal); Methodology (equal); Software (equal); Validation (equal); Writing – original draft (lead). **F. Zeighami:** Conceptualization (supporting); Data curation (equal); Formal analysis (equal); Methodology (equal); Software (equal); Validation (equal); Writing – original draft (equal). **A. Palermo:** Conceptualization (equal); Methodology (equal); Writing – review & editing (equal). **C. Daraio:** Conceptualization (equal); Resources (lead); Writing – review & editing (supporting).

DATA AVAILABILITY

The data that support the findings of this study are available from the corresponding author upon reasonable request.

REFERENCES

[1]M. Eichenfield, J. Chan, R. M. Camacho, K. J. Vahala, and O. Painter, "Optomechanical crystals," Nature **462**, 78–82 (2009).
[2]J. R. Raney, N. Nadkarni, C. Daraio, D. M. Kochmann, J. A. Lewis, and K. Bertoldi, "Stable propagation of mechanical signals in soft media using stored elastic energy," Proc. Natl. Acad. Sci. U. S. A. **113**, 9722–9727 (2016).
[3]M. Sigalas, M. S. Kushwaha, E. N. Economou, M. Kafesaki, I. E. Psarobas, and W. Steurer, "Classical vibrational modes in phononic lattices: Theory and experiment," Z. Kristallogr. Cryst. Mater. **220**, 765–809 (2005).
[4]S. Benchabane, A. Khelif, J.-Y. Rauch, L. Robert, and V. Laude, "Evidence for complete surface wave band gap in a piezoelectric phononic crystal," Phys. Rev. E **73**, 065601 (2006).
[5]Y. Achaoui, A. Khelif, S. Benchabane, L. Robert, and V. Laude, "Experimental observation of locally-resonant and Bragg band gaps for surface guided waves in a phononic crystal of pillars," Phys. Rev. B **83**, 104201 (2011).
[6]O. B. Wright and O. Matsuda, "Watching surface waves in phononic crystals," Philos. Trans. R. Soc., A **373**, 20140364 (2015).
[7]A. Palermo, Y. Wang, P. Celli, and C. Daraio, "Tuning of surface-acoustic-wave dispersion via magnetically modulated contact resonances," Phys. Rev. Appl. **11**, 044057 (2019).
[8]F. Zeighami, A. Palermo, D. Bogomolov, and A. Marzani, "Experimental investigation of Rayleigh wave propagation in a locally resonant metamaterial layer resting on an elastic half-space," APL Mater. **12**, 021115 (2024).
[9]A.-C. Hladky-Hennion and M. D. Billy, "Experimental validation of band gaps and localization in a one-dimensional diatomic phononic crystal," J. Acoust. Soc. Am. **122**, 2594–2600 (2007).
[10]N. Boechler, G. Theocharis, S. Job, P. G. Kevrekidis, M. A. Porter, and C. Daraio, "Discrete breathers in one-dimensional diatomic granular crystals," Phys. Rev. Lett. **104**, 244302 (2010).
[11]N. Boechler, G. Theocharis, and C. Daraio, "Bifurcation-based acoustic switching and rectification," Nat. Mater. **10**, 665–668 (2011).
[12]Y. Pennec, B. Djafari-Rouhani, H. Larabi, J. O. Vasseur, and A. Hladky-Hennion, "Low-frequency gaps in a phononic crystal constituted of cylindrical dots deposited on a thin homogeneous plate," Phys. Rev. B **78**, 104105 (2008).
[13]Y. Jin, Y. Pennec, B. Bonello, H. Honarvar, L. Dobrzynski, B. Djafari-Rouhani, and M. I. Hussein, "Physics of surface vibrational resonances: Pillared phononic crystals, metamaterials, and metasurfaces," Rep. Prog. Phys. **84**, 086502 (2021).
[14]Y.-F. Wang, V. Laude, and Y.-S. Wang, "Coupling of evanescent and propagating guided modes in locally resonant phononic crystals," J. Phys. D: Appl. Phys. **47**, 475502 (2014).
[15]A. Khelif, Y. Achaoui, S. Benchabane, V. Laude, and B. Aoubiza, "Locally resonant surface acoustic wave band gaps in a two-dimensional phononic crystal of pillars on a surface," Phys. Rev. B **81**, 214303 (2010).
[16]A. Colombi, V. Ageeva, R. Smith, A. Clare, R. Patel, M. Clark, D. Colquitt, P. Roux, S. Guenneau, and R. Craster, "Enhanced sensing and conversion of ultrasonic Rayleigh waves by elastic metasurfaces," Sci. Rep. **7**, 6750 (2017).
[17]Z. Lin and S. Tol, "Elastic metasurfaces for full wavefront control and low-frequency energy harvesting," J. Vib. Acoust. **143**, 061005 (2021).
[18]L. Cao, Z. Yang, Y. Xu, S.-W. Fan, Y. Zhu, Z. Chen, B. Vincent, and B. Assouar, "Disordered elastic metasurfaces," Phys. Rev. Appl. **13**, 014054 (2020).
[19]L. Cao, Z. Yang, Y. Xu, Z. Chen, Y. Zhu, S.-W. Fan, K. Donda, B. Vincent, and B. Assouar, "Pillared elastic metasurface with constructive interference for flexural wave manipulation," Mech. Syst. Sig. Process. **146**, 107035 (2021).
[20]L. Virgin and R. Plaut, "Postbuckling and vibration of linearly elastic and softening columns under self-weight," Int. J. Solids Struct. **41**, 4989–5001 (2004).
[21]COMSOL Multiphysics®, "COMSOL AB," (Stockholm, Sweden, 2025).
[22]D. Bigoni, F. Bosi, D. Misseroni, F. Dal Corso, and G. Noselli, "New phenomena in nonlinear elastic structures: From tensile buckling to configurational forces," in *Extremely Deformable Structures* (Springer, 2015), pp. 55–135.
[23]A. K. Chopra, *Dynamics of Structures* (Pearson Education India, 2007).
[24]A. Palermo, M. Vitali, and A. Marzani, "Metabarriers with multi-mass locally resonating units for broad band Rayleigh waves attenuation," Soil Dyn. Earthquake Eng. **113**, 265–277 (2018).
[25]I. The MathWorks, "MATLAB function reference: Fsolve," (accessed July 23, 2025).
[26]A. Palermo, S. Krödel, A. Marzani, and C. Daraio, "Engineered metabarrier as shield from seismic surface waves," Sci. Rep. **6**, 39356 (2016).
[27]K. F. Graff, *Wave Motion in Elastic Solids* (Courier Corporation, 2012).
[28]L. Rayleigh, "On waves propagated along the plane surface of an elastic solid," Proc. London Math. Soc. **17**(s1), 4–11 (1885).
[29]D. Colquitt, A. Colombi, R. Craster, P. Roux, and S. Guenneau, "Seismic metasurfaces: Sub-wavelength resonators and Rayleigh wave interaction," J. Mech. Phys. Solids **99**, 379–393 (2017).